# Differential regulation of systemic arterial pressure by the skin: role of HIF isoforms

Andrew S. Cowburn[1,2,3], Norihiko Takeda[3], Adam T. Boutin[3], Jung-whan Kim[3], Jane Sterling[2], Manando Nakasaki[3], Mark Southwood[5], Ananda W. Goldrath[3], Colin Jamora[3], Victor Nizet[4], Edwin Chilvers[2], and Randall S. Johnson[1]

Department of Physiology, Development and Neuroscience[1], Department of Medicine[2], University of Cambridge; Department of Pathology, Papworth Hospital NHS Foundation Trust[5]; Division of Biological Sciences[3], Department of Pediatrics and Skaggs School of Pharmacy and Pharmaceutical Sciences[4], University of California, San Diego

For correspondence:
Rsj33@cam.ac.uk

**Vascular flow through tissues is regulated via a number of homeostatic mechanisms. Localized control of tissue blood flow, or autoregulation, is a key factor in regulating tissue perfusion and oxygenation. We show here that the net balance between two HIF transcription factor isoforms, HIF-1α and HIF-2α is an essential mechanism regulating both local and systemic blood flow in the skin of mice. We show here that HIF isoform balance in keratinocyte-specific mutant mice affects thermal adaptation, exercise capacity, and systemic arterial pressure. The two primary HIF isoforms do this in opposing ways, and this is associated with HIF isoform regulation of nitric oxide (NO) production. We also show a correlation exists between altered levels of HIF isoforms in the skin, and the degree of idiopathic hypertension in human subjects. Thus, the balance between HIF-1α and HIF-2α expression in keratinocytes is a novel control element of both tissue perfusion, and systemic arterial pressure, with potential implications in human hypertension.**

\body

Introduction

Autoregulation of vascular flow in peripheral tissues is essential for controlling both local tissue perfusion and for the regulation of systemic blood pressure. This dual role for peripheral blood flow is in turn dependent on a range of factors that act to adjust local vascular tone. A key element of this control is the balance between $O_2$ demand and $O_2$ supply(1). This balance causes increased need for oxygen to induce increased blood flow. This regulatory pathway in peripheral tissues has a direct impact on systemic arterial pressure, because peripheral vascular resistance determines in large part total vascular resistance in the arterial bed.

The skin contains a very extensive series of vascular plexi. This vascular bed has a range of essential functions, which include regulating body temperature. Skin circulation is also altered in a number of disease states, including renal disease(2), hypercholesterolemia(3), peripheral vascular disease(4), heart failure and hypertension(5). Identification of structural alterations to the subcutaneous microvasculature provides a powerful prognostic tool to predict cardiovascular events in hypertensive patients(6), and impaired microvascular vasodilation and capillary rarefaction is associated with familial predisposition to hypertension(7).

The heterodimeric transcription factors hypoxia-inducible factor HIF-1$\alpha$ and HIF-2$\alpha$ are essential for the maintenance of cellular oxygen homeostasis(8). In response to hypoxia, stabilized HIF-1$\alpha$ and HIF-2$\alpha$ proteins initiate the expression of genes that alleviate hypoxic stress, including genes promoting cell growth, adhesion and migration, new vessel formation and the development of vascular networks(9, 10).

Recent data from a number of groups has indicated that HIF-1$\alpha$ and HIF-2$\alpha$ can act in a dualistic manner to regulate a range of responses in vivo; these interactions include functionally opposing interactions with the Myc transcription factors(11-13), with the tumor suppressor p53(14-16), and with mTOR(17).

Work by Prabhakar and co-workers showed that HIF-1$\alpha$ and HIF-2$\alpha$ global heterozygosity influenced ventilatory rates and thus a number of responses to

oxygenation controlled by the carotid body(18-20). They have now extended this work to show that there is also a functional antagonism between the HIF isoforms that regulates cardiorespiratory homeostasis through the carotid body and adrenal medulla (21). This work connects HIF isoform balance and the global control of response to physiological oxygenation.

We have previously shown that in macrophages, nitric oxide (NO) homeostasis can be regulated differentially through the opposing transcriptional effects of Th1 and Th2 cytokines on HIF-1$\alpha$ and HIF-2$\alpha$, respectively(22). NO is a key regulator of vascular tone(23) and the physiological importance of NO in the regulation of blood pressure is highlighted by the fact that pharmacological inhibition of NO synthases leads to severe hypertension(24).

Here we perform a detailed analysis of the role that HIF isoform balance plays in the regulation of nitric oxide equilibrium in the skin. Our results indicate that this balance in oxygen responsive transcription factor isoforms is a key factor in the overall maintenance of systemic arterial pressures; and that an alteration in this balance correlates with idiopathic hypertension in human subjects.

## Results

To characterize how HIF might function as a modulator of NO and thereby influence tissue vascular autoregulation, with the skin as a model peripheral tissue, we utilized mouse strains with conditional alleles of the relevant HIF$\alpha$ isoforms crossed to mouse strains expressing Cre recombinase under the control of the keratin 14 (K14) promoter. This experimental platform drives the excision of the HIF$\alpha$ isoforms only where the K14 promoter is active, i.e., within basal layers of the epidermis. Of interest, keratinocyte deletion of HIF-2$\alpha$ induced greater HIF-1$\alpha$ stability in the skin when compared to wt control, possibly suggesting some sort of compensatory mechanism. This phenomenon was not reciprocated in the K14cre-HIF-1$\alpha$ with regards to HIF-2$\alpha$ expression (fig. S1).

HIF-1$\alpha$ has a key role in NOS2 regulation in response to Th1 cytokines(25-27), and, as shown previously, HIF-2$\alpha$ has a similarly important role in the

regulation of arginase-1, in a Th2-cytokine-dependent fashion(22). In macrophages HIF-1α-dependent expression of NOS2 results in increased NO, via increased L-arginine utilization, whereas depletion of L-arginine via enhanced arginase activity stimulated by HIF-2α induction of the arginase-1 gene acts to reduce available L-arginine. This alternative utilization of L-arginine reduces the availability of this substrate for NO synthases, and thus indirectly reduces NO production(22).

To determine whether this pattern of differential HIF-1α/HIF-2α regulation of NO homeostasis also occurs in keratinocytes, independently of cytokine stimulation, we analyzed both RNA (fig. 1A) and protein (fig. 1B) isolated from skin biopsies of K14cre-HIFα mice. These show a marked reduction in the expression of NOS2 mRNA and protein in K14cre-HIF-1α mice when compared to littermate controls. In contrast, K14cre-HIF-2α mice show marked reduction in mRNA and protein of both arginase-1 and -2 expression (fig. 1A-B), with representative Western blots shown in fig. S2A.

While analysis of plasma nitrates revealed little variation in basal concentrations between mutant mice and their littermate controls (fig. 1C) measurement of skin nitrate levels revealed that K14cre-HIF-2α mutant mice accumulated far greater concentrations of nitrates than littermate controls (0.96μM, for control animals and 3.83μM for K14cre-HIF-2α mutant mice n=9, $p<0.05$) and K14cre-HIF-1α mutants (0.88μM, n=9)(fig. 1D). Mass spectrometric analysis of free soluble amino acids extracted from the skin of K14cre-HIF-1α mice showed a significant increase in arginine (with non-significant changes in ornithine and proline), suggesting alterations in arginine utilization in the skin of these mice (fig. 1E). Another prominent NO synthase, NOS1, appeared to be have a minimal level of expression in skin, and its expression was unaffected in the mutants (fig. S2B). Together these observations indicate that the HIF pathway is a significant regulator of arginine utilization through known HIF targets such as NOS2/iNOS.

Initial histological analysis suggested a normal development of skin architecture, with no abnormalities in the development of dermal blood vessels in any of the K14cre-HIF-α mutant mice when compared to non-transgenic littermate controls (fig. S3A), even though VEGF gene expression

trended lower in K14cre-HIF-1α (fig. S3B). Quantification identified a vascular density of between 2.5-3% across the mutant and control animals (fig. 2A). However, micro-vascular diameters were significantly reduced in the K14cre-HIF-1α mutant mice when compared to littermate controls (fig. 2B and fig. S3C).

Loss of epidermal HIF-1α did not affect either core body or skin temperatures, however, loss of HIF-2α significantly increased both core-body (wt 37.05±0.09$^{o}$C, HIF-2α mutant 37.47±0.06$^{o}$C, $p<0.005$, n=15-29) and skin temperatures (wt 34.62±0.22$^{o}$C, HIF-2α mutant 35.35±0.10$^{o}$C, $p<0.05$, n=17-33) when compared to wt littermate controls (fig. 2C-D). Furthermore, loss of epidermal HIF-2α significantly increased basal metabolism relative to that of littermate controls or K14cre-HIF-1α mice (fig. S4A-B)

Given the effects of deletion of the HIF-α isoforms on skin and core temperatures, a temperature conservation challenge was used to determine whether the mechanisms for core body preservation in the cold were affected in these mutants. K14cre-HIF-2α mice quickly became hypothermic relative to littermate control mice, with a significant defect in acclimation evident 3hr after the onset of cold stress (4$^{o}$C) (wt 35.5$^{o}$C n=9, HIF-2α mutant 34.6$^{o}$C n=6, $p<0.05$) (fig. 2E). Epidermal deletion of HIF-1α did not influence acclimation to cold environmental temperatures. There was a significant difference between the two isoform knockout animals, where again each deviated in opposing directions from the wild type core temperature.

To further probe heat dissipation through the skin and determine whether HIF isoforms in keratinocytes had opposing effects on this vital physiological process, control and mutant mice were subjected to strenuous exercise, where significant defects were observed in attaining a high $VO_2$ max in both HIF-1α and HIF-2α keratinocyte mutants (fig. S4C-D). If this was due to defects in heat dissipation through the skin(28), a higher core temperature should result from defective vasodilation, and a lower core temperature from excessive cutaneous vasodilation. This is in fact what was seen: as shown in figure 2F, loss of cutaneous HIF-1α resulted in a significant elevation of core temperature post-exercise relative to wild type controls (wt 37.51±0.21$^{o}$C, mutant 37.96±0.08$^{o}$C, $p<0.05$, n=6). Furthermore, thermo-imaging pre- and

post-exercise revealed lower skin temperatures in the tails of K14cre-HIF-1α mice post-exercise when compared to littermate controls (fig. 2G-H). These data indicate that the loss of either HIF-1α or HIF-2α in keratinocytes affects the systemic adaptive mechanisms required for heat dissipation, again, in opposing fashions.

As a key negative regulator of HIFα protein stability, the tumor suppressor Von Hippel-Lindau factor was examined for its effects on heat dissipation. Interestingly, in these mutants, the resultant increase in expression of both HIF isoforms resulted in mice with greatly reduced skin temperatures (fig. S5A-C, as well as profound defects in adaptation to cold challenge, and metabolism (fig. S5D-E).

One of the most important measures of alterations in peripheral vascular resistance is an alteration in systemic arterial pressure. Basal blood pressure was thus recorded for K14cre-HIF-α isoform mutants (fig. 3A): Keratinocyte deletion of HIF-1α (n=20) gave rise to a significantly increased systolic (122mm/Hg vs 111mm/Hg) and diastolic (98mm/Hg vs 91mm/Hg) pressure, i.e., induced hypertension (HTN) relative to control mice (n=34). In contrast, HIF-2α (n=10) deletion in keratinocytes significantly lowered basal systolic (103mm/Hg) and diastolic (82mm/Hg) pressures, causing systemic hypotension.

A number of markers of cardiac stress are known to be associated with HTN. To examine this more closely, mRNA was isolated from the heart tissue of controls and keratinocyte deletion HIF-α isoform mutants, and analyzed for the expression of Nppa (natriuretic peptide A), Nppb (natriuretic peptide B), Acta1 (actin alpha 1 skeletal muscle) and myh7 (myosin heavy chain 7 cardiac muscle), a selection of genes recognized to be transcriptionally up-regulated in cardiac tissue from hypertensive subjects(29, 30). All four genes were increased in cardiac tissue from K14cre-HIF-1α mice (fig. 3B), verifying cardiac stress secondary to induced HTN. Deletion of keratinocyte HIF-2α (fig. 3B) showed a trend towards lowered expression profiles of these same markers in cardiac tissue.

As cardiac tissue also shows fibrotic changes in hypertension, we examined ventricular walls for fibrosis in mutants, and found that fibrotic areas were

significantly greater in the hypertensive K14cre-HIF-1α mutants relative to that seen in controls (fig. 3C). Of note, biochemical analysis of blood samples from K14cre-HIF-1α show normal liver and kidney function when compared to wt control (table S1).

To explore how differential keratinocyte HIF-α isoform expression might influence vascular tension during HTN, an acute HTN syndrome was induced in mutant and control mice via a 14 day infusion of angiotensin-II (Ang-II) (2μg/Kg/min) through a surgically implanted osmotic mini-pump(31). Mean systolic (158mm/Hg vs 111mm/Hg, $p<0.01$) and diastolic (111mm/Hg vs 89mm/Hg, $p<0.01$) blood pressures were significantly increased at day 14 in Ang-II treated wild type mice compared to vehicle controls (fig. S6A).

In K14cre-HIF-1α mutant mice (n=7) there was a significant increase in both systolic (187mm/Hg vs 170mm/Hg) and diastolic (138mm/Hg vs 119mm/Hg) blood pressures when compared to littermate controls (fig. 4A). Here again, the opposite effect on blood pressure was seen in K14cre-HIF-2α mutant mice (n=7) where substantial protection against Ang-II induced hypertension was seen, with a attenuation in both systolic and diastolic blood pressures (fig. 4A). The percentage of cardiac fibrotic tissue was also significantly less in the K14cre-HIF-2α mutants when compared to litter mate controls (fig. 4B-C). This indicates that loss of HIF-2α in the skin has an ameliorating effect on the severe hypertension induced in this model.

Analysis of RNA isolated from the skin of K14cre-HIF-1α mice identified no deviation in the expression of NOS2, or arginase-1 or –2 when compared to similarly treated (Ang-II) wild type controls (fig. 4D). Conversely, K14cre-HIF-2α mice demonstrated a significant increase in NOS2 gene expression (8.01±2.0 fold change, n=6, $p<0.05$)(fig. 4D). This observation was confirmed by a significant increase in skin-associated nitrate concentration (7.8±1μM vs 5.0±0.5μM respectively, n=4, $p<0.05$)(fig. 4E). There was a reduction of skin nitrate isolated from K14cre-HIF-1α mice (n=4, $p=0.06$), here again showing an opposite effect from the effect caused by the deletion of the HIF-2α isoform. Of interest, a number of recent studies have documented a heightened interaction/stability of HIF-1α in angiotensin-II treated animals(32) we observed a significant and coordinate increase in both HIF-1α and HIF-2α

proteins in the skin of wild type control mice treated with Ang II (fig. 4F-G), as well as in increase in the expression of NOS2. The expression of NOS1 mRNA (fig. S6B) and NOS3 protein remained unchanged (fig 4F).

This last observation indicates that HIF isoform expression is modulated in wild type mice by the induction of hypertension. Although intriguing, and clearly supportive of an essential role of HIF isoform balance in the maintenance of the appropriate peripheral vascular resistance in mice, we wished to determine how this might relate to human hypertensive disease. To ascertain relevance to human HTN, we recruited consenting subjects that were either normotensive or had established mild HTN (and who were otherwise healthy) as volunteers for skin biopsy analysis of HIF-$\alpha$ expression. Ethical approval was obtained from the local Research Ethics Committee (Ref:11/EE/0028). Volunteers were screened for HTN status, age, and medication, as shown in Table S2.

Initial blood pressure measurements confirmed the hypertensive state of the subjects, with significantly higher systolic (154mm/Hg vs 126mm/Hg, $p<0.005$), diastolic (89mm/Hg vs 73mm/Hg, $p<0.005$) and mean arterial blood pressures (110 mm/Hg vs 91mm/Hg, $p<0.005$) in the hypertensive group (n=16) compared to healthy normal controls (n=24) respectively (fig. 5A). A determination of nitrate levels in these subjects also showed that hypertension was correlated with a significantly decreased amount of skin nitrate (fig. 5B) with a strong trend towards a reduction in NOS2 gene expression (fig. S7). Immunohistochemical analysis of epidermal HIF-$\alpha$ isoform expression showed that decreased expression of HIF-1$\alpha$ in the epidermal layer correlated significantly with increased mean blood pressure; while increased epidermal HIF-2$\alpha$ expression, specifically nuclear localization of HIF-2$\alpha$ correlated very significantly with increased mean blood pressure. These data suggest again opposing roles of the HIF$\alpha$ isoforms on peripheral vascular resistance and, ultimately, blood pressure (fig. 5C-D).

## Discussion

Regulation of blood flow distribution through vascular beds is achieved through complex adjustments of the vascular tone, and thus the resistance of

the microcirculation to blood flow. HIF are expressed in a wide range of tissue types, and as oxygen responsive modulators of vascular function, they act as agents that respond to different levels of tissue perfusion. The two main HIF-α factors have a number of both overlapping and divergent gene targets; but recent evidence has indicated that they can act to co-regulate important biological control pathways through functionally oppositional targets. We report here evidence that a balance of HIF-1α and HIF-2α in the skin is essential for controlling peripheral vascular resistance. We have previously shown that inflammatory cytokines can influence the balance of HIF-1α and HIF-2α, and that this in turn regulates macrophage production of NO via differential regulation of the HIF target genes iNOS/NOS2 and arginase1(22). Our data indicate that this pathway for control of NO homeostasis also exists in keratinocytes, although in this case in the absence of cytokine regulation. In this peripheral and highly vascularized tissue, it is a localized mechanism for control of vascular flow.

Vasodilation induced by nitric oxide is known to act as a physiological counterbalance to the vasoconstriction controlled by both the sympathetic nervous system and by renin-angiotensin action. It is clear that NO is a key regulator of peripheral vascular resistance: blockade of NO synthesis with inhibitory L-arginine analogues has been shown to increase peripheral vasoconstriction(33, 34), and increase systemic blood pressure(33, 35). A number of studies have also linked nitric oxide bioavailability with endothelial cell dysfunction and hypertension(36, 37). Hypertensive subjects have lower serum levels of bioavailable NO than normotensive controls(37, 38), and increasing the availability of L-arginine, the natural substrate of NOS, leads to heightened vasodilation and decreases in arterial blood pressure(39, 40). Of note, differences in NOS2 expression and activity have been found between mouse and human cells, with a number of discrepancies between tissue types questioning, how much NOS2 contributes to the metabolism of L-arginine in humans (1,2). We further report discrepancies on NOS2 expression in human keratinocyte. Given the influence angiotensin-II had on murine keratinocyte NOS2 expression, the theoretical variance was not replicated in mild

hypertensive human volunteers. Further work is required to determine the tissue specific contribution of NOS2 and arginase-1/2 to the generation of NO. Increased peripheral vascular resistance in the skin can lead to alterations in vascular density, and ultimately to vascular rarefaction. The arginase enzymes, which are shown here to be induced by HIF-2α, are not only important because they can indirectly influence NO generation; they are also critical in channeling L-arginine to L-ornithine, and ultimately, for the production of the polyamines and L-proline. These in turn contribute to increased collagen synthesis, which is itself linked to fibrosis. Thus, an aberrant spectrum of HIF isoform function/expression may underlie many of the fibrotic vascular pathologies evident in patients with hypertension.

These data show that hypertensive individuals differentially express HIF-1α and HIF-2α, with a loss of the concordant regulation evident in normotensives. We demonstrated previously that deletion of the HIF negative regulator VHL in keratinocytes can act to disturb vascular flow to other organs, including to the viscera (12). This alteration in vascular flow has striking physiological effects, including changes in synthesis of erythropoietin at distant sites. Clearly, the overall regulation of NO homeostasis in tissue beds via oxygen responsive factors is a potent mechanism to accomplish physiological balance, apart from the traditional axes of this control, i.e., the kidney and central nervous system. Previous studies of Prabhakar and co-workers (19, 21) reported the partial global deletion of HIF-2α influenced a number of physiological parameters including the hypertensive status of these mice. The crucial disparity between our data and those previously reported is the tissue specificity of the HIF-α deletion. The overall physiological influence of HIF-α appears to dependent not only on isoform dominance but also on tissue specific expression. Future work to determine how altered differential expression of HIF-1α and HIF-2α occurs in hypertension should also illuminate how differences in the regulation of these isoforms, both in skin and potentially in other tissue beds, can be induced by the initiating events of hypertension.

## Materials and methods

*Animals.* All animals were housed in an association and accreditation of laboratory animal care international-approved facility, and animal experiments were conducted in accordance with the National Institute of Health guide for the care and use of laboratory animals.
Targeted deletion of HIF-1$\alpha$ and HIF-2$\alpha$ in keratinocytes was created by crossing mice (C57Bl6/j) homozygous for the floxed allele in HIF-1$\alpha$, HIF-2$\alpha$ or VHL into a background of Cre recombinase expression driven by the K14 promoter, which is specific to cells of the keratinocyte linage.

*Metabolic analysis.* Energy expenditure of the K14-mutant mice and their wild-type littermates was measured using the Columbus Instruments Oxymax system according to the manufacturers instructions. For exercise tolerance testing, mice were allowed to acclimatize to the enclosed treadmill environment for 15 min prior to stimulation. The treadmill was initiated at 5m/min increasing to 9, 12, 15 and 18m/min on a 15$^{o}$ incline. $VO_2$ was measure every 30 sec on a 150 sec cycle before the speed of the treadmill was increased.

*Mouse temperatures and blood pressure analysis.* Surface temperatures were measured with a FLIR Thermovision A20 thermal infrared camera and image data analyzed using FLIR image analysis software. All core body temperatures were taken rectally with a TEGRAM 871A digital thermometer (Braintree Scientific Inc) using a RET-1 rectal probe. Temperature acclimation tests were conducted in bare cages with water and food supplied ad lib. Rectal temperature were taken before and every hour up to 6hr. Blood pressure was monitored in restrained conscious mice by the tail-cuff occlusion method, according to the manufacturers instructions (Coda systems, Kent Scientific, USA). This method of blood pressure analysis has been extensively validated. Repeat measurements using tail-cuff occlusion have been shown to closely match radiotelemetry analysis. (41)

*Immunofluorescence and quantification of vascular density and vascular diameter.* Mouse skin isolated from wild-type and K14cre animals were frozen in OCT (Tissue-Tek). Staining for the epidermal basal layer marker K5, MAC-1, CD31 (BD PharMingen) was performed on 8-μm frozen sections after the tissues were fixed for 10 min in 4% paraformaldehyde or acetone (for CD31). Images were acquired on an Olympus Bx51 microscope with an Olympus DP70 camera. Acquisition was performed using a 40× 1.3 UPlan FL N objective (Olympus). For quantitation of vascular density in the skin, CD31 staining was calculated as a percentage of dermal area by ImageJ software (NIH). Results are from five random fields using a 10x objective and normalized against the wild-type value. To assess vessel diameter, confocal microscopic images of the skin were acquired using a LSM 700 fitted with an Axio Observer.Z1 (Carl Zeiss). The blood vessels were only examined in an area of the dermis within a 100mm distance from the epidermal-dermal junction. The diameters of blood vessels were measured by ImageJ software (NIH). Results are from five random fields using a 40x objective.

*Cardiac fibrosis analysis.* Formalin-fixed paraffin-wax embedded hearts were sectioned (4μm) and collagen deposition was assessed on Sirius red–stained sections. Image analysis was performed using imageJ software (NIH).

*RNA analysis.* Total RNA was isolated from skin, lung, heart and liver using TRI-reagent (Sigma) followed by RNA clean-up and DNase digest using RNeasy column kits (Qiagen). First-strand synthesis was performed with 1μg of total RNA using a high-capacity cDNA kit (Applied Biosystems) according to the manufacturers instructions. Relative gene expression was determined by qPCR (ABI Prism 7700 sequence detection system, Applied Biosystems) and amplified in Sybr-green master mix (Applied Biosystems) and relevant primers from Qiagen. Relative gene expression levels were related to β-actin using the $2^{-CT}$ method. Relative gene expression in human skin were related to YWHAZ expression.

*Immunoblotting.* Tissue samples were lysed in RIPA buffer. A total of 50μg of whole cell lysates were loaded on to a 4-12% Bis-Tris gels from Invitrogen

(NuPAGE®). The primary antibodies used in this study were: rabbit polyclonals anti-HIF-1α anti-HIF-2α (1:1000, Novus Biologicals), anti-NOS2, anti-NOS3, anti-arginase-II (1:200, Santa Cruz Biotechnology) mouse monoclonal anti-arginase-I (1:1000, Santa Cruz Biotechnology). Secondary antibodies used were: goat anti-rabbit IgG-HRP (1:2000, RnD systems) and rabbit anti-mouse IgG-HRP (1:5000, GE Healthcare).

*Nitric oxide analysis.* Blood samples were centrifuged to separate plasma, and passed through a column with a 10kDa cut-off filter. Skin $NO_{(X)}$ were isolated from 500mg of homogenized tissue using a hypotonic lysis buffer and centrifuged (1000*g*, 4$^{o}$C, 5mins). All samples were analyzed for total NO(x) content using a NOA 280i (Siever, GE Healthcare) according to the manufacturers instructions.

*Angiotensin II induced hypertension model.* Angiotensin II (or vehicle control) was administered through an osmotic mini-pump (Model 2002, Alzet, Cupertino, CA) implanted subcutaneously to deliver 2μg/Kg/min over a 14 day time period.

*Human Skin Biopsy.* Small elliptical skin biopsies were carefully removed from the lateral abdominal wall of 33 consenting healthy volunteers at the Addenbrooke's University of Cambridge teaching Hospital NHS Foundation Trust, Cambridge UK. Ethical approval was obtained from the local Research Ethics Committee (Ref:11/EE/0028). Participants consisted of 16 subjects with previously diagnosed mild hypertensive and 17 normotensive subjects. The relevant participant details are presented in supplementary table 1. All skin biopsy samples collected were divided into two and rapidly snap frozen in $LN_2$ for RNA and protein.

*Human skin immunohistochemistry.* Formalin-fixed paraffin-wax embedded skin biopsies were sectioned (4μm) and incubated with monoclonal mouse anti-human HIF1α (1:100) and polyclonal rabbit anti-human HIF2α (1:200) (both Novus Biologicals, USA). Antibodies were detected using 3,3'-

diaminobenzidine tetrahydrochloride to create a brown reaction product, counterstained with haematoxylin (Dako, UK) and examined by light microscopy. Quantification was performed by imageJ software (NIH).

*Statistic analysis.* All data represent the mean (±SEM) of (*n*) separate experiments unless otherwise stated. Differences between groups were assessed using *t-test* unless otherwise stated. A *p* value of <0.05 was considered significant.

Figure legends

**Figure 1.** Molecular and cellular characterization of mice with keratinocyte specific deletion of HIF-1α or HIF-2α. (**A**) Baseline qPCR and (**B**) Western blot analysis of HIFα target genes expressed in skin samples from keratinocyte specific HIF-1α (grey bar), or HIF-2α (closed bar) deleted mice compared to wild-type controls (open bars). Data shown are mean fold change ± SEM and mean protein AU ± SEM for qPCR and Western blots respectively (n=8). Baseline NO(x) analysis in (**C**) plasma and (**D**) skin samples from the same K14cre-HIF-1α, K14cre-HIF-2α and wild-type control mice described in (**A-B**) above. Data shown are mean μM ± SEM and μM/mg of tissue ± SEM (n=9). (**E**) Analysis of soluble amino acid fraction in skin extracts from K14cre-HIF-1α (n=3) compared to wt controls (n=3)

**Figure. 2.** Keratinocyte specific deletion of HIFα influences skin vascular diameter and thermoregulation. (**A**) Histological analysis of vascular density; ImageJ software (NIH) was used for quantitative analysis to determine the percentage vessel density. Sections were analyzed from 10-12 week old K14cre-HIF-1α, K14cre-HIF-2α and K14cre- HIF-1α/HIF-2α and compared to non-transgenic littermate controls (n=4). Data shown percentage CD31 positive staining ± SEM. (**B**) Histological analysis of vascular diameter, ImageJ software (NIH) was used for quantitative analysis to determine the vessel cross-section. Sections were analyzed from K14cre-HIF-1α, K14cre-HIF-2α, and compared to non-transgenic littermate controls (n=4), Data shown as mean vessel diameter (μM) ± SEM. (**C**) Basal core body and (**D**) skin temperature were analysed in K14cre-HIF-1α, HIF2α and wt mice (data shown as mean $^{o}$C ± SEM, n=15-33). (**E**) Core-body temperature was monitored during acclimation of K14cre-HIF-1α, K14cre-HIF-2α to 4$^{o}$C environmental temperature compared to wild-type controls. Data shown as mean drop in core temperature ($^{o}$C) ± SEM following 3h exposure (n=6-9). (**F**) Core body temperature ($^{o}$C) was measured pre- and post-exercise to determine the dissipation of heat (n=6). (**G-H**) Tail skin temperature was monitor pre and post exercise stress. Thermal infrared imaging suggested HIF-1α mutant mice dissipate significantly less thermal energy through tail

skin than wild-type mice (data shown as mean ($^{o}$C) ± SEM)(n=5). (*p<0.05, **p<0.005).

**Figure. 3.** Murine keratinocyte expression of HIF-1α /-2α subunits modulates systemic blood pressure (**A**) Blood pressure was measured non-invasively through tail-cuff occlusion. Data shown are average values of 10 independent readings in 8-10 week-old wild-type (n=34), K14cre-HIF-1α (n=20) and K14cre-HIF-2α (n=10) mice, and displayed as systolic and diastolic values ± SEM. (**B**) Relative mRNA levels of Nppa, Acta1, Myh7 and Nppb (genes known to be influenced by hypertension) in cardiac tissue was determined by qPCR from resting wt (open bar, n=3) K14cre-HIF-1α (grey bar, n=3) and K14cre-HIF-2α (closed bar, n=3) mice. (**C**) Baseline cardiac fibrosis was determined in K14cre-HIF-1α (8-10 week old) compared to wild-type (n=5). Histological sections were stained with sirrus red, quantified by imageJ software (NIH) and displayed as percentage collagen in total fields ± SEM. (*p<0.05, **p<0.005).

**Figure. 4.** Epidermal deletion of HIF-2α drives skin NOS2 expression and reduces cardiac fibrosis in an angiotensin-II induced hypertension model. Wild-type and mutant K14cre mice received a constant infusion of angiotensin II (2mg/Kg/day) or vehicle control via a subcutaneously inserted osmotic pump. (**A**) Blood pressure was measured by tail-cuff occlusion on day 0 (dissecting line) and day14 (bar). Data shown are average values of 10 independent readings from wt (n=7) K14cre-HIF-1α (n=7) and K14cre-HIF-2α (n=7). (**B**-**C**) Cardiac fibrosis was determined in wt, K14cre-HIF-1α (n=4) and K14cre-HIF-2α (n=4) 14 days post osmotic pump insertion. Histological sections of the left ventricle were stained with sirrus red and quantified by imageJ software (NIH). Representative photomicrographs demonstrate the remarkable contrast in collagen deposition. (**D**) QPCR analysis of NOS2, Arginase-I and Arginase-II mRNA from the skin of wt (open bar, n=6), K14cre-HIF-1α (grey bar, n=6) and K14cre-HIF-2α (closed bar, n=6) 14 days post osmotic pump insertion. (**E**) Total nitric oxide was determined in skin lysates by the conversion of NO(x) to NO using a Nitric Oxide Analyser (Siever). Data shown are mean (μM/mg tissue) ± SEM from wt (n=4) K14cre-HIF-1α (n=4)

and K14cre-HIF-2α (n=4) 14 days post osmotic pump insertion. (**F**-**G**) Protein analysis of skin samples show an increase in expression of both HIF-1α and HIF-2α with a corresponding increase of both NOS2 and arginase-I (data shown as mean (AU) ± SEM, n=4). (**G**) Representative photomicrographs of Western blots are shown.

**Figure. 5.** Expression pattern of HIF-1α and HIF-2α in the skin of normotensive and hypertensive subjects. (**A**) Sphygmomanometer measurements of volunteer blood pressure. Normotensive (closed circles, n=24) and hypertensive (closed triangle, n=16) dot plots are divided into systolic, diastolic and arterial mean blood pressure. (**B**) Total nitric oxide was determined in skin lysates by the conversion of NO(x) to NO using a Nitric Oxide Analyser (Siever). Data shown are mean (μM/mg tissue) ± SEM. Normotensives shown as open bar (NT, n=17) and hypertensive subjects as closed bar (HT, n=10). (**C**) Linear regression analysis of human skin IHC stained for HIF-1α or HIF-2α (percentage positive signal in squamous epithelial layer) compared to mean BP (mm/Hg). HIF-1α produced a significant correlation (closed circles, $r^2$=0.2057, p=0.0340, n=22), HIF-2α also produced a significant correlation (open square, $r^2$=0.3580, p=0.0033, n=22). (*p<0.05, **p<0.005). (**D**) Representative photomicrographs of histological analysis for human skin HIF-1α and HIF-2α expression.

**Figure. S1.** Representative Western blots and densitometry analysis for HIF-1α and HIF-2α stability in skin samples from K14cre-HIF2α and K14cre-HIF-1α mice respectively when compared to wt controls. Densitometry data are ratio of target protein against β-actin and shown as mean± SEM (n=6)

**Figure. S2.** (A) Representative Western blots of arginase-I /-II, NOS2 /3 and b-actin control basally expressed in the skin of K14cre-HIF1α, HIF2α compared to littermate controls. (B) Baseline qPCR analysis for NOS1 expression in skin samples from keratinocyte specific HIF-1α and HIF-2α deleted mice compared to wt controls. Data shown are mean fold change ± SEM (n=8).

**Figure. S3.** (A) Representative photomicrographs of histological analysis for

skin vascular density. Frozen 8 μM skin sections were immunostained for PCAM-1 (CD31). ImageJ software (NIH) was used for quantitative analysis to determine the percentage vessel density. (B) Baseline qPCR analysis for VEGF expression in skin samples from keratinocyte specific HIF-1a and HIF-2a deleted mice compared to wild-type controls. Data shown are mean fold change± SEM (n=8). (C) Representative photomicrographs of histological analysis of vascular diameter. Frozen 8 μM skin sections were immunostained for PCAM-1 (CD31). ImageJ software (NIH) was used for quantitative analysis to determine the vessel cross-section.

**Figure. S4.** Metabolic characterization of K14cre-HIF-1α and K14cre-HIF-2α. Measurement of $VO_2$ and $VCO_2$ from resting (A) K14cre-HIF-1$\alpha$ or (B) K14cre-HIF-2$\alpha$ mice (data shown as mean $VO_2$ or $VCO_2$ ± SEM ml/Kg/hr), respiratory exchange ration (RER) (data shown as mean ratio ± SEM) and metabolic heat production (data shown as mean Kcal/Kg/h ± SEM) (n=5) (*$p<0.05$, **$p<0.005$). (C and D) Whole-body $O_2$ consumption ($VO_2$) in response to accumulating exercise stress. (C) K14-HIF-1α (n=5) or (D) K14-HIF-2α (n=5) were compared to littermate controls (n=4) (anova **$p<0.005$). Data shown are mean $VO_2$ ± SEM ml/Kg/hr accumulating with time as the intensity of the exercise increases.

**Figure. S5.** K14cre-VHL mice are hypothermic. (A-B) Skin surface temperature was measured by a thermal infrared camera and expressed as average temperature ($^oC$) ± SEM (n=8). (C) Core-body temperature was monitored during acclimation of K14cre-VHL to 4$^oC$ environmental temperature compared to wild-type controls. Data shown as the mean drop in core temperature ($^oC$) ± SEM following 3h exposure (n=8). Measurement of VO2 and VCO2 from resting K14cre-VHL mice (Data shown as mean $VO_2$ or $VCO_2$ ± SEM ml/Kg/hr), metabolic heat production (Data shown as mean Kcal/Kg/h ± SEM) (n=8)(**$p<0.005$)

**Figure. S6.** Angiotensin II (2ug/kg/min) infusion in wt over 14 days drives hypertension. WT mice develop severe hypertension (data shown as mean (mm/Hg) ± SEM, n=6).

**Figure. S7.** QPCR analysis of NOS1, NOS2, NOS3 and VEGF from skin samples collected from normotensive (open bar n=11) and mildly hypertensive (closed bar n=13) volunteers. Data shown are mean fold change ± SEM.

**Table. S1.** Murine blood chemistry analysis, comparing K14cre-HIF1$\alpha$ with littermate control (n=10)

**Table. S2.** Human volunteer data. Subjects are divided into Normotensive and hypertensive subjects


1. Duling BR & Klitzman B (1980) Local control of microvascular function: role in tissue oxygen supply. *Annu Rev Physiol* 42:373-382.
2. Stewart J*, et al.* (2004) Noninvasive interrogation of microvasculature for signs of endothelial dysfunction in patients with chronic renal failure. *Am J Physiol Heart Circ Physiol* 287(6):H2687-2696.
3. Khan F, Litchfield SJ, Stonebridge PA, & Belch JJ (1999) Lipid-lowering and skin vascular responses in patients with hypercholesterolaemia and peripheral arterial obstructive disease. *Vasc Med* 4(4):233-238.
4. Rossi M & Carpi A (2004) Skin microcirculation in peripheral arterial obliterative disease. *Biomed Pharmacother* 58(8):427-431.
5. Green DJ*, et al.* (2006) Impaired skin blood flow response to environmental heating in chronic heart failure. *Eur Heart J* 27(3):338-343.
6. De Ciuceis C*, et al.* (2007) Structural alterations of subcutaneous small-resistance arteries may predict major cardiovascular events in patients with hypertension. *American journal of hypertension* 20(8):846-852.
7. Noon JP*, et al.* (1997) Impaired microvascular dilatation and capillary rarefaction in young adults with a predisposition to high blood pressure. *J Clin Invest* 99(8):1873-1879.
8. Semenza GL (2007) Oxygen-dependent regulation of mitochondrial respiration by hypoxia-inducible factor 1. *Biochem J* 405(1):1-9.
9. Pouyssegur J, Dayan F, & Mazure NM (2006) Hypoxia signalling in cancer and approaches to enforce tumour regression. *Nature* 441(7092):437-443.
10. Semenza GL (2003) Targeting HIF-1 for cancer therapy. *Nat Rev Cancer* 3(10):721-732.
11. Gordan JD, Bertout JA, Hu CJ, Diehl JA, & Simon MC (2007) HIF-2alpha promotes hypoxic cell proliferation by enhancing c-myc transcriptional activity. *Cancer Cell* 11(4):335-347.
12. Boutin AT*, et al.* (2008) Epidermal sensing of oxygen is essential for systemic hypoxic response. *Cell* 133(2):223-234.
13. Dang CV, Kim JW, Gao P, & Yustein J (2008) The interplay between MYC and HIF in cancer. *Nat Rev Cancer* 8(1):51-56.

14. Ravi R, *et al.* (2000) Regulation of tumor angiogenesis by p53-induced degradation of hypoxia-inducible factor 1alpha. *Genes Dev* 14(1):34-44.
15. Bertout JA, *et al.* (2009) HIF2alpha inhibition promotes p53 pathway activity, tumor cell death, and radiation responses. *Proc Natl Acad Sci U S A* 106(34):14391-14396.
16. Roberts AM, *et al.* (2009) Suppression of hypoxia-inducible factor 2alpha restores p53 activity via Hdm2 and reverses chemoresistance of renal carcinoma cells. *Cancer Res* 69(23):9056-9064.
17. Brugarolas J, *et al.* (2004) Regulation of mTOR function in response to hypoxia by REDD1 and the TSC1/TSC2 tumor suppressor complex. *Genes Dev* 18(23):2893-2904.
18. Kline DD, Peng YJ, Manalo DJ, Semenza GL, & Prabhakar NR (2002) Defective carotid body function and impaired ventilatory responses to chronic hypoxia in mice partially deficient for hypoxia-inducible factor 1 alpha. *Proc Natl Acad Sci U S A* 99(2):821-826.
19. Peng YJ, *et al.* (2011)Hypoxia-inducible factor 2alpha (HIF-2alpha) heterozygous-null mice exhibit exaggerated carotid body sensitivity to hypoxia, breathing instability, and hypertension. *Proc Natl Acad Sci U S A* 108(7):3065-3070.
20. Nanduri J, *et al.* (2009) Intermittent hypoxia degrades HIF-2alpha via calpains resulting in oxidative stress: implications for recurrent apnea-induced morbidities. *Proc Natl Acad Sci U S A* 106(4):1199-1204.
21. Yuan G, *et al.* (2013) Mutual antagonism between hypoxia-inducible factors 1alpha and 2alpha regulates oxygen sensing and cardio-respiratory homeostasis. *Proc Natl Acad Sci U S A* 110(19):E1788-1796.
22. Takeda N, *et al.* (2010) Differential activation and antagonistic function of HIF-{alpha} isoforms in macrophages are essential for NO homeostasis. *Genes Dev* 24(5):491-501.
23. Boegehold MA (2010) Endothelium-dependent control of vascular tone during early postnatal and juvenile growth. *Microcirculation* 17(5):394-406.
24. Qiu C, Muchant D, Beierwaltes WH, Racusen L, & Baylis C (1998) Evolution of chronic nitric oxide inhibition hypertension: relationship to renal function. *Hypertension* 31(1):21-26.
25. Nagai M, *et al.* (2011) Role of blood cell-associated angiotensin II type 1 receptors in the cerebral microvascular response to ischemic stroke during angiotensin-induced hypertension. *Exp Transl Stroke Med* 3:15.
26. Munder M, Eichmann K, & Modolell M (1998) Alternative metabolic states in murine macrophages reflected by the nitric oxide synthase/arginase balance: competitive regulation by CD4+ T cells correlates with Th1/Th2 phenotype. *J Immunol* 160(11):5347-5354.
27. Melillo G, *et al.* (1995) A hypoxia-responsive element mediates a novel pathway of activation of the inducible nitric oxide synthase promoter. *J Exp Med* 182(6):1683-1693.
28. Carter R, 3rd, Wilson TE, Watenpaugh DE, Smith ML, & Crandall CG (2002) Effects of mode of exercise recovery on thermoregulatory and cardiovascular responses. *J Appl Physiol* 93(6):1918-1924.

29. Marques FZ, Campain AE, Yang YH, & Morris BJ (2010) Meta-analysis of genome-wide gene expression differences in onset and maintenance phases of genetic hypertension. *Hypertension* 56(2):319-324.
30. Ye P & West MJ (2003) Cosegregation analysis of natriuretic peptide genes and blood pressure in the spontaneously hypertensive rat. *Clin Exp Pharmacol Physiol* 30(12):930-936.
31. Vital SA, Terao S, Nagai M, & Granger DN (2010) Mechanisms underlying the cerebral microvascular responses to angiotensin II-induced hypertension. *Microcirculation* 17(8):641-649.
32. Sanchez-Lopez E*, et al.* (2005) Angiotensin II regulates vascular endothelial growth factor via hypoxia-inducible factor-1alpha induction and redox mechanisms in the kidney. *Antioxidants & redox signaling* 7(9-10):1275-1284.
33. Vecchione C*, et al.* (2009) Pressure-induced vascular oxidative stress is mediated through activation of integrin-linked kinase 1/betaPIX/Rac-1 pathway. *Hypertension* 54(5):1028-1034.
34. Qiu C, Engels K, Samsell L, & Baylis C (1995) Renal effects of acute amino acid infusion in hypertension induced by chronic nitric oxide blockade. *Hypertension* 25(1):61-66.
35. Vecchione C*, et al.* (2005) Protection from angiotensin II-mediated vasculotoxic and hypertensive response in mice lacking PI3Kgamma. *J Exp Med* 201(8):1217-1228.
36. Mason RP*, et al.* (2009) Loss of arterial and renal nitric oxide bioavailability in hypertensive rats with diabetes: effect of beta-blockers. *American journal of hypertension* 22(11):1160-1166.
37. Hermann M, Flammer A, & Luscher TF (2006) Nitric oxide in hypertension. *J Clin Hypertens (Greenwich)* 8(12 Suppl 4):17-29.
38. Ghasemi A, Zahediasl S, Syedmoradi L, & Azizi F (2011) Association between serum nitric oxide metabolites and hypertension in a general population. *International angiology : a journal of the International Union of Angiology* 30(4):380-387.
39. Dong JY*, et al.* (2011) Effect of oral L-arginine supplementation on blood pressure: a meta-analysis of randomized, double-blind, placebo-controlled trials. *American heart journal* 162(6):959-965.
40. Gokce N (2004) L-arginine and hypertension. *The Journal of nutrition* 134(10 Suppl):2807S-2811S; discussion 2818S-2819S.
41. Feng M*, et al.* (2008) Validation of volume-pressure recording tail-cuff blood pressure measurements. *American journal of hypertension* 21(12):1288-1291.

(1) Vitek MP, et al, (2001) Characterization of NO and cytokine production in immune-activated microglia and peritoneal macrophages derived from a mouse model expressing the human NOS2 gene on a mouse NOS2 knockout background. *Antioxid Redox Signal* 8(5-6): 893-901.

(2) Bronte V, & Zanovello P. (2005) Regulation of immune responses by L-arginine metabolism. *Nature Reviews Immunology* 5 (8): 641-654.

**Figure. 1**

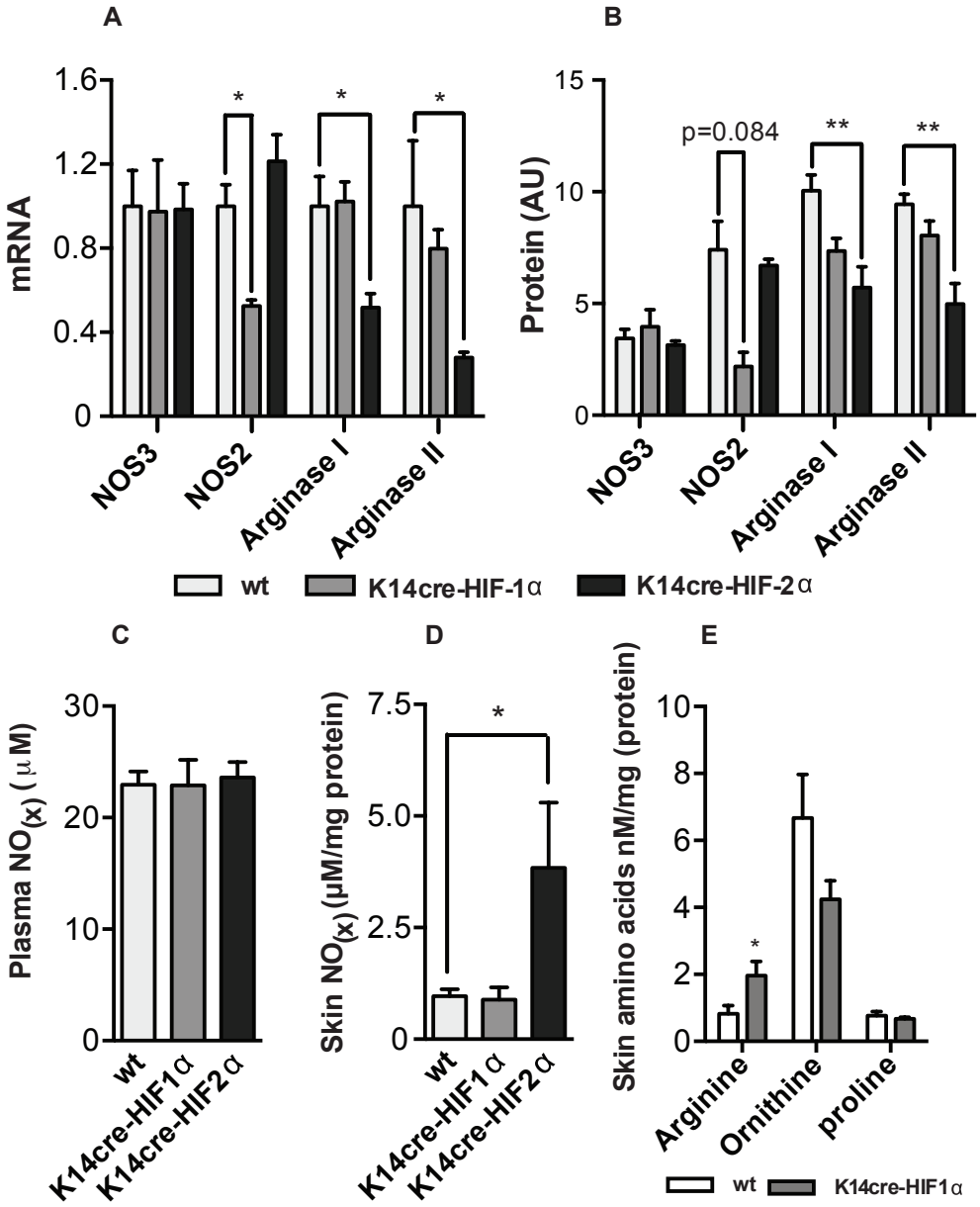
A
B
mRNA
Protein (AU)
1.6
1.2
0.8
0.4
0
15
10
5
0
*
*
*
p=0.084
**
**
NOS3
NOS2
Arginase I
Arginase II
wt
K14cre-HIF-1α
K14cre-HIF-2α
C
D
E
Plasma NO(x) (μM)
Skin NO(x) (μM/mg protein)
Skin amino acids nM/mg (protein)
30
20
10
0
7.5
5.0
2.5
0
10
8
6
4
2
0
*
*
wt
K14cre-HIF1α
K14cre-HIF2α
Arginine
Ornithine
proline
wt
K14cre-HIF1α

Figure. 2

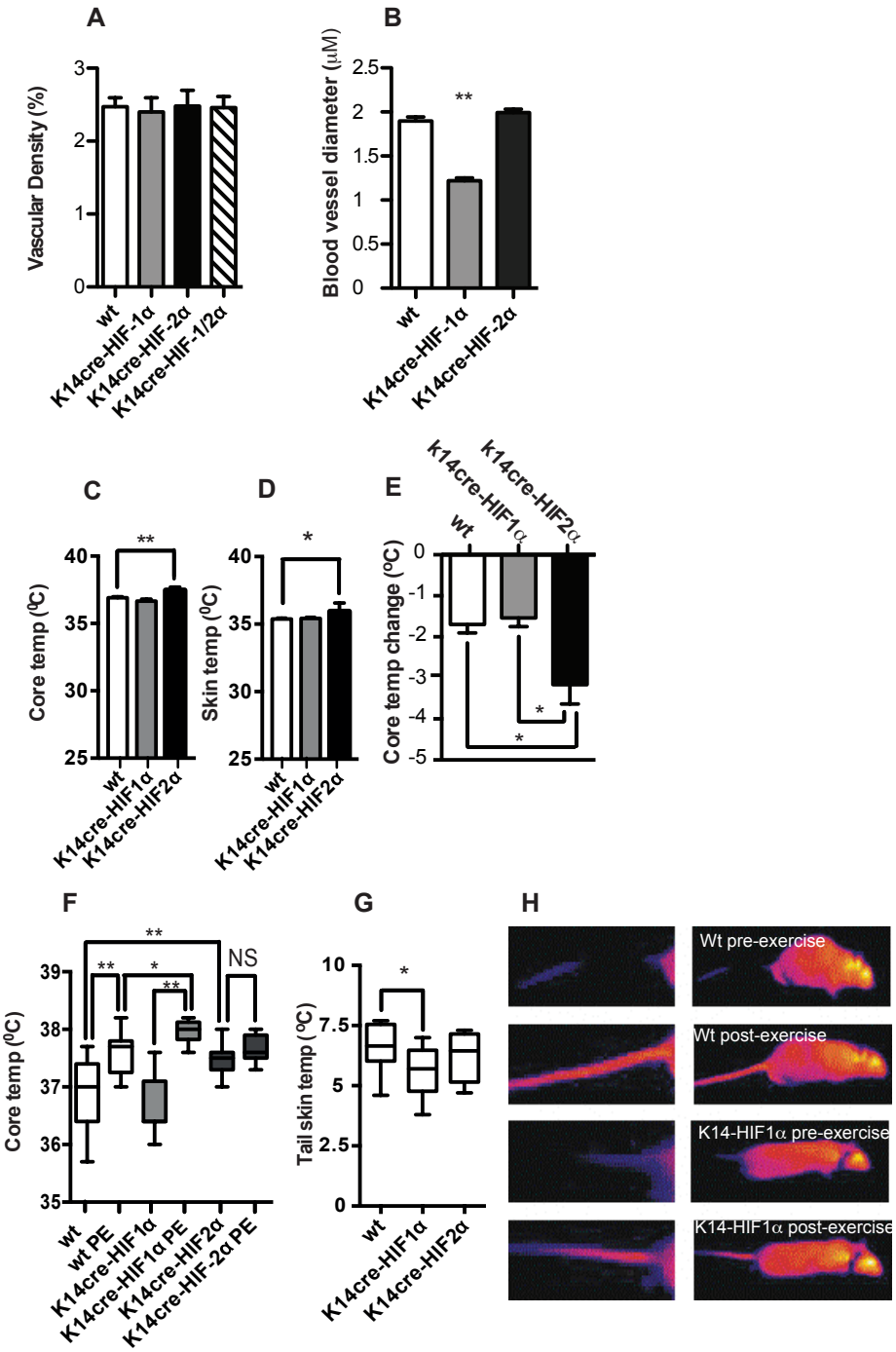
A
Vascular Density (%)
3
2
1
0
wt
K14cre-HIF-1α
K14cre-HIF-2α
K14cre-HIF-1/2α
B
Blood vessel diameter (μM)
2.5
2
1.5
1
0.5
0
**
wt
K14cre-HIF-1α
K14cre-HIF-2α
C
Core temp (⁰C)
40
35
30
25
**
wt
K14cre-HIF1α
K14cre-HIF2α
D
Skin temp (⁰C)
40
35
30
25
*
wt
K14cre-HIF1α
K14cre-HIF2α
E
wt
K14cre-HIF1α
K14cre-HIF2α
Core temp change (⁰C)
0
-1
-2
-3
-4
-5
*
*
F
Core temp (⁰C)
39
38
37
36
35
**
**
*
**
NS
wt
wt PE
K14cre-HIF1α
K14cre-HIF1α PE
K14cre-HIF2α
K14cre-HIF-2α PE
G
Tail skin temp (⁰C)
10
7.5
5
2.5
0
*
wt
K14cre-HIF1α
K14cre-HIF2α
H
Wt pre-exercise
Wt post-exercise
K14-HIF1α pre-exercise
K14-HIF1α post-exercise

**Figure. 3**

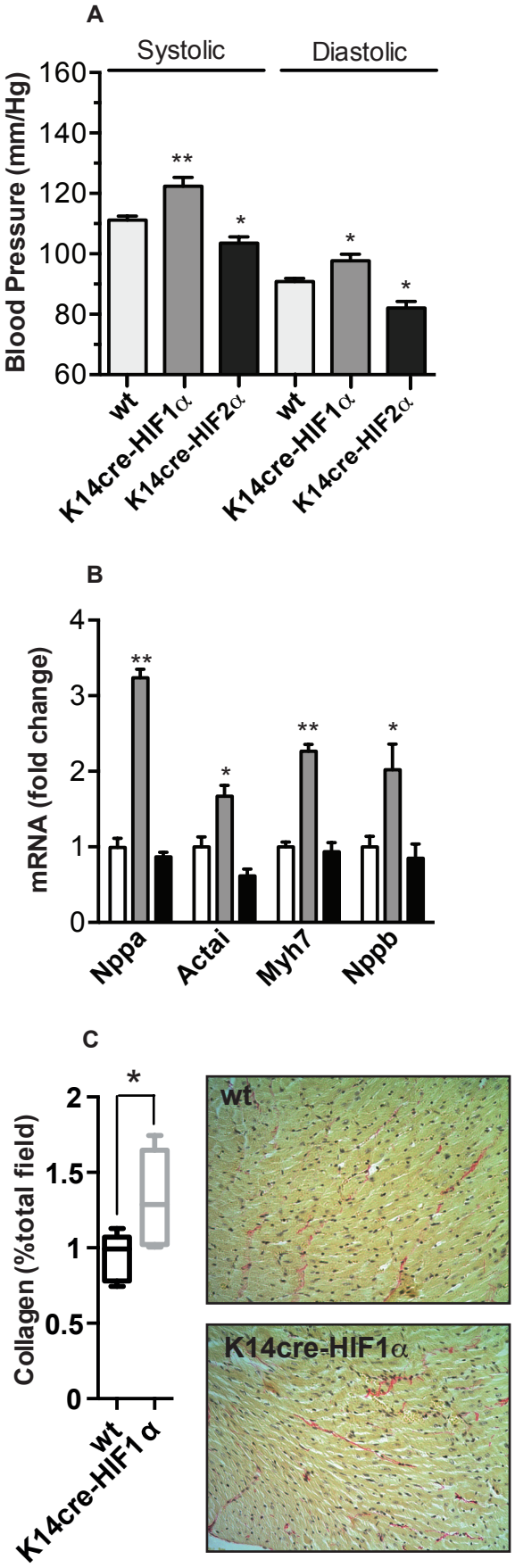
A
Systolic
Diastolic
Blood Pressure (mm/Hg)
160
140
120
100
80
60
**
*
*
*
wt
K14cre-HIF1α
K14cre-HIF2α
wt
K14cre-HIF1α
K14cre-HIF2α
B
mRNA (fold change)
4
3
2
1
0
**
*
**
*
Nppa
Actai
Myh7
Nppb
C
Collagen (%total field)
2
1.5
1
0.5
0
*
wt
K14cre-HIF1α
wt
K14cre-HIF1α

Figure. 4

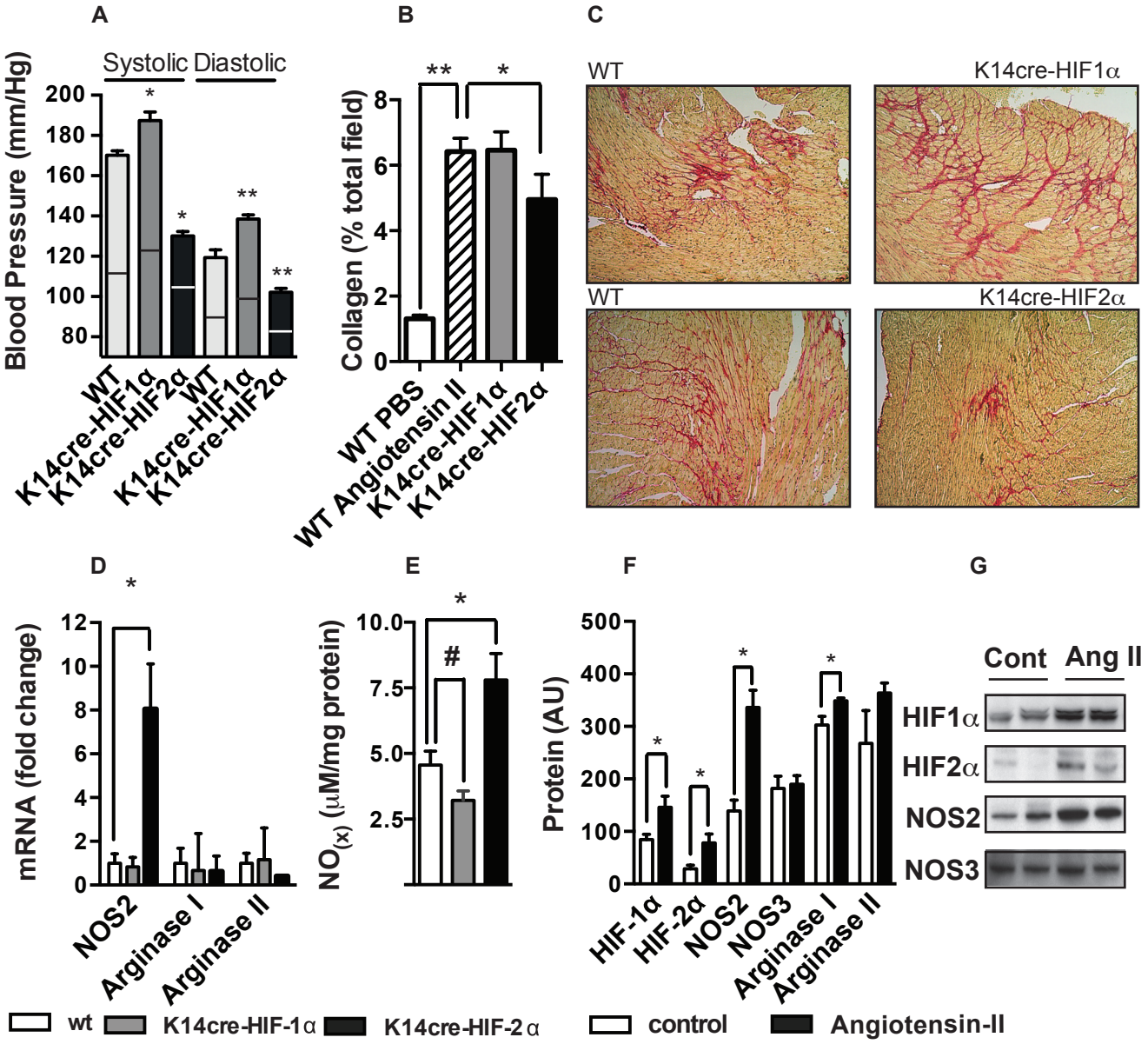
A
Systolic Diastolic
Blood Pressure (mm/Hg)
200
180
160
140
120
100
80
WT
K14cre-HIF1α
K14cre-HIF2α
WT
K14cre-HIF1α
K14cre-HIF2α
B
Collagen (% total field)
8
6
4
2
0
WT PBS
WT Angiotensin II
K14cre-HIF1α
K14cre-HIF2α
C
WT
K14cre-HIF1α
WT
K14cre-HIF2α
D
mRNA (fold change)
12
10
8
6
4
2
0
NOS2
Arginase I
Arginase II
E
NO(x) (μM/mg protein)
10.0
7.5
5.0
2.5
F
Protein (AU)
500
400
300
200
100
0
HIF-1α
HIF-2α
NOS2
NOS3
Arginase I
Arginase II
G
Cont
Ang II
HIF1α
HIF2α
NOS2
NOS3
wt
K14cre-HIF-1α
K14cre-HIF-2α
control
Angiotensin-II

Figure. 5.

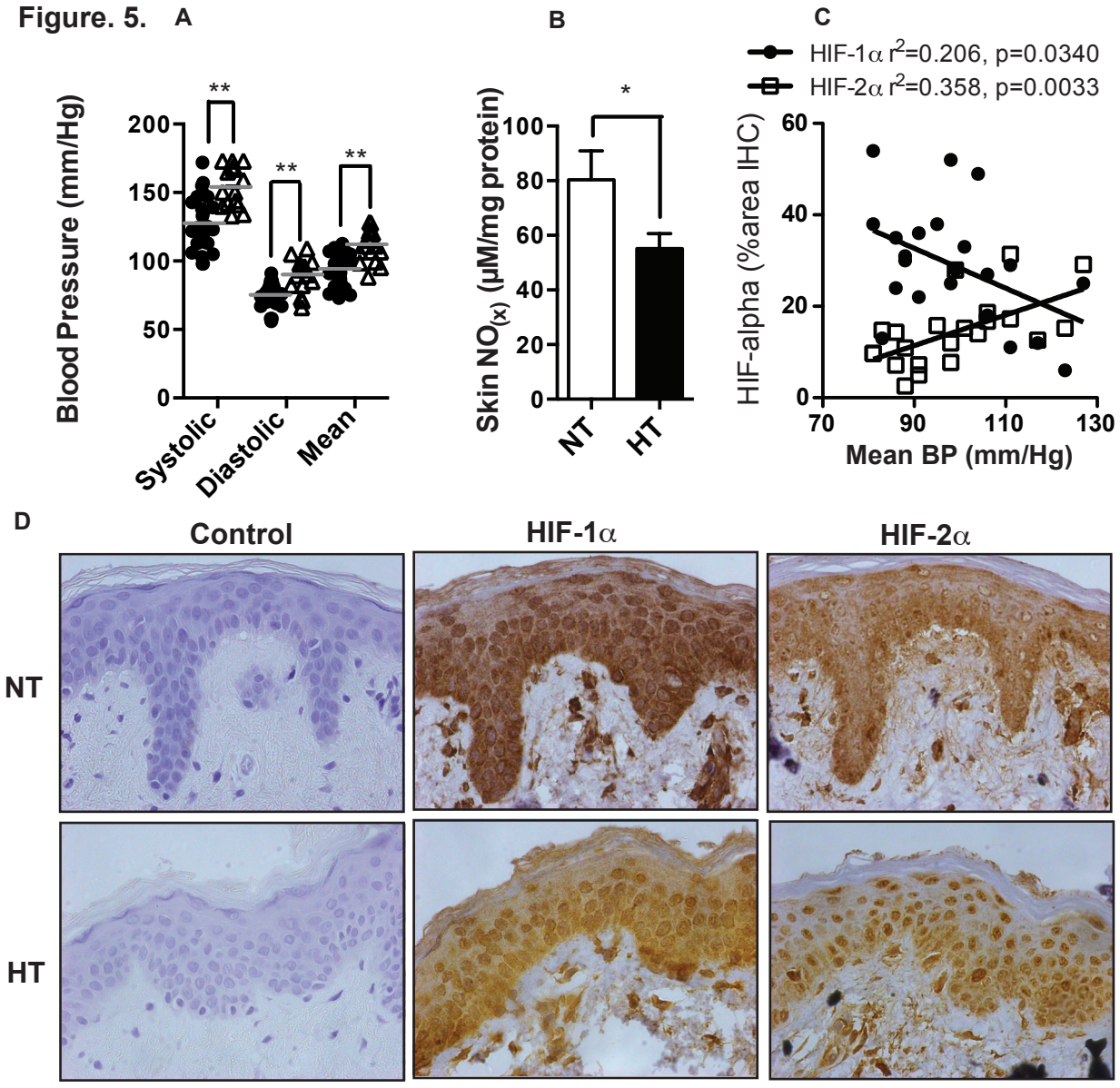
A
B
C
Blood Pressure (mm/Hg)
200
150
100
50
0
**
**
**
Systolic
Diastolic
Mean
Skin NO(x) (μM/mg protein)
100
80
60
40
20
0
*
NT
HT
HIF-1α r2=0.206, p=0.0340
HIF-2α r2=0.358, p=0.0033
HIF-alpha (%area IHC)
60
40
20
0
70
90
110
130
Mean BP (mm/Hg)
D
Control
HIF-1α
HIF-2α
NT
HT

Fig. S1

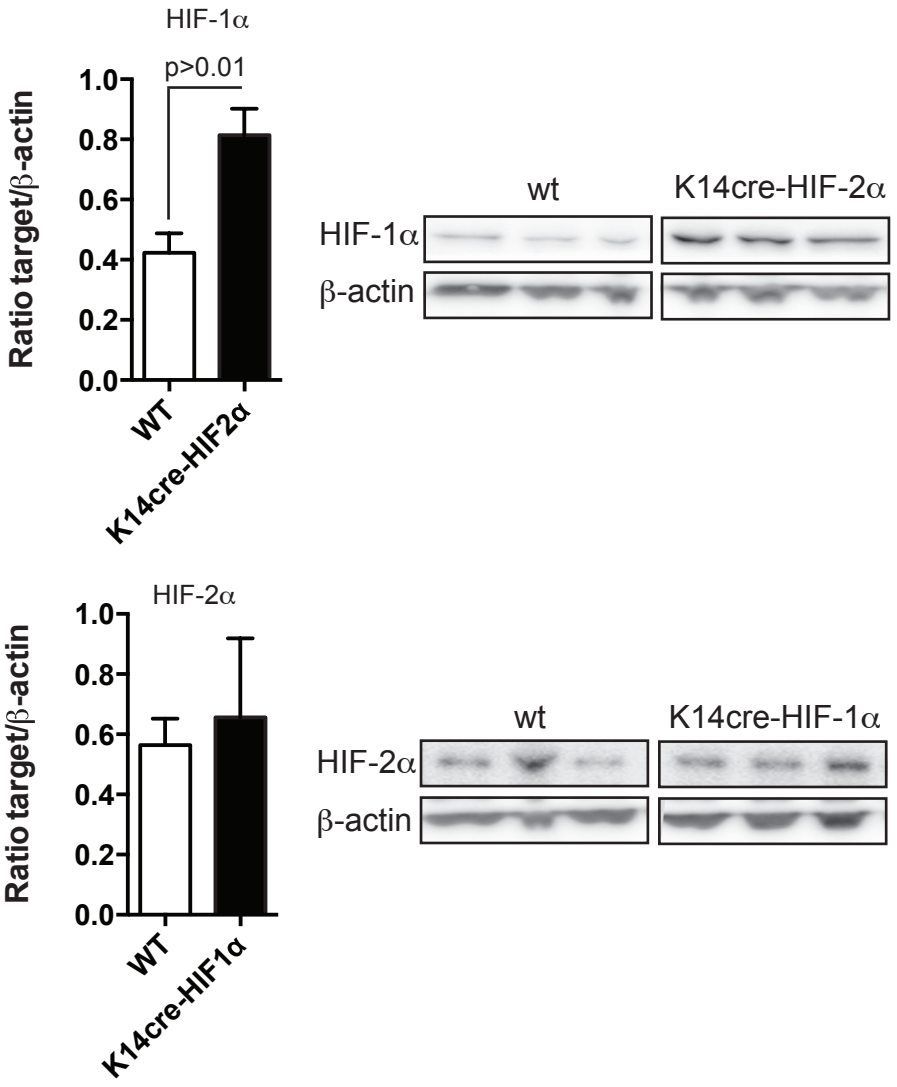


**Figure. S1.** Representative Western blots and densitometry analysis for HIF-1α and HIF-2α stability in skin samples from K14cre-HIF2α and K14cre-HIF-1α mice respectively when compared to wt controls. Densitometry data are ratio of target protein against β-actin and shown as mean± SEM (n=6)

Fig S2

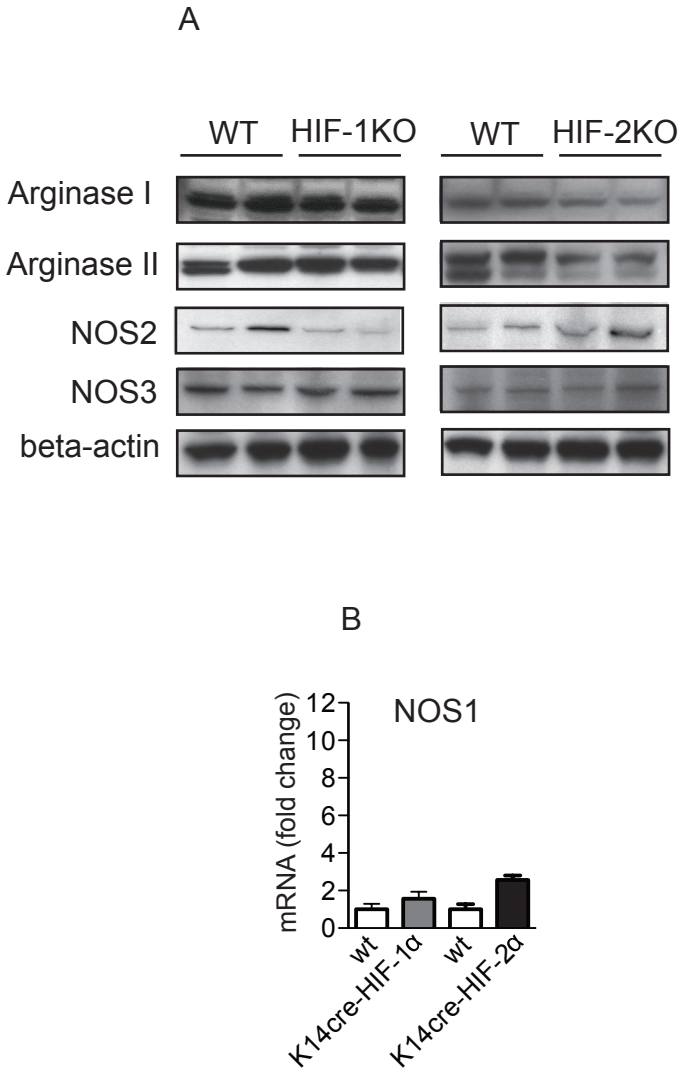


**Figure S2**. (A) Representative Western blots of arginase-I /-II, NOS2 /3 and β-actin control basally expressedin the skin of K14cre-HIF1α, HIF-2α compared to littermate controls. (B) Baseline qPCR analysis for NOS1 expression in skin samples from keratinocyte specific HIF-1α and HIF-2α deleted mice compared to wild-type controls. Data shown are mean fold change ± SEM (n=8).

Fig. S3

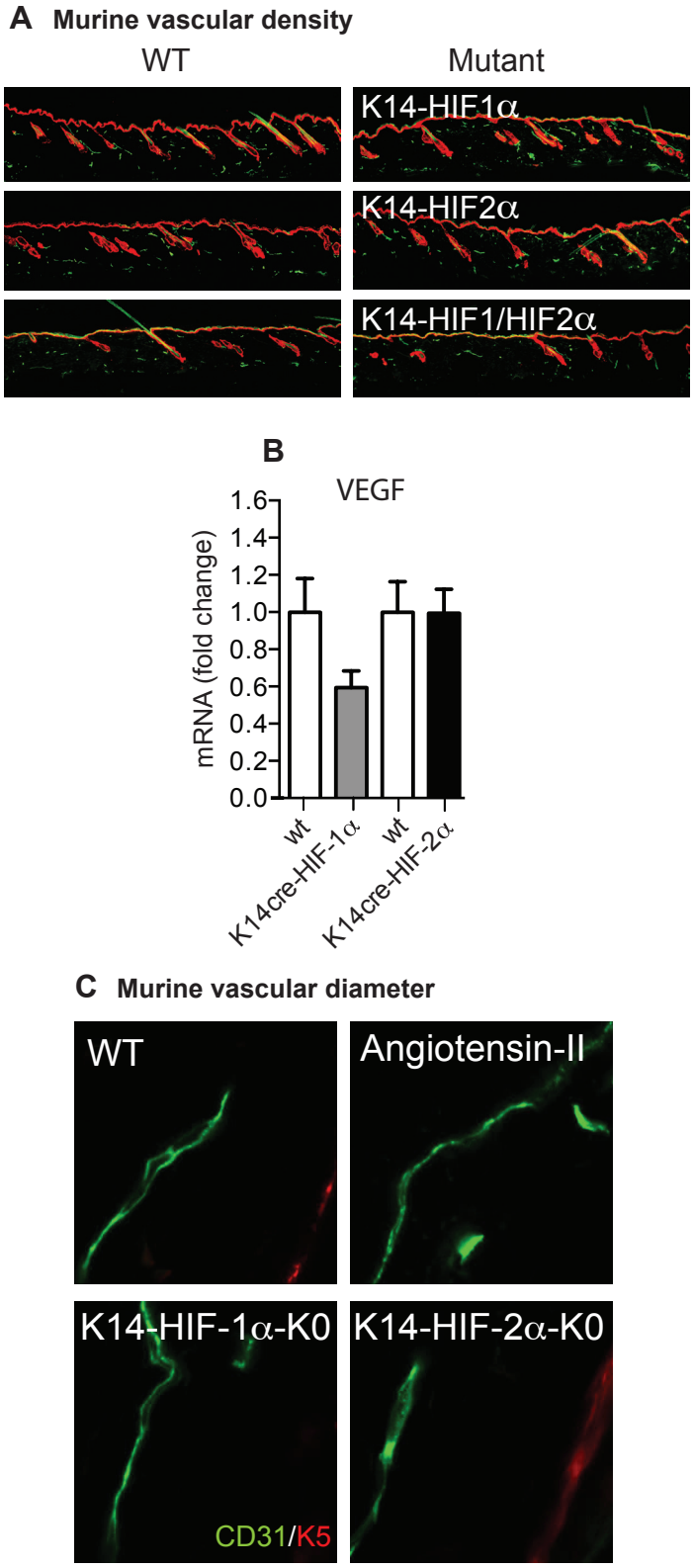


**Figure. S3.** (A) Representative photomicrographs of histological analysis for skin vascular density. Frozen 8 μM skin sections were immunostained for PCAM-1 (CD31). ImageJ software (NIH) was used for quantitative analysis to determine the percentage vessel density. (B) Baseline qPCR analysis for VEGF expression in skin samples from keratinocyte specific HIF-1α and HIF-2α deleted mice compared to wild-type controls. Data shown are mean fold change ± SEM (n=8).
(C) Representative photomicrographs of histological analysis of vascular diameter. Frozen 8 μM skin sections were immunostained for PCAM-1 (CD31). ImageJ software (NIH) was used for quantitative analysis to determine the vessel cross-section.

Fig. S4

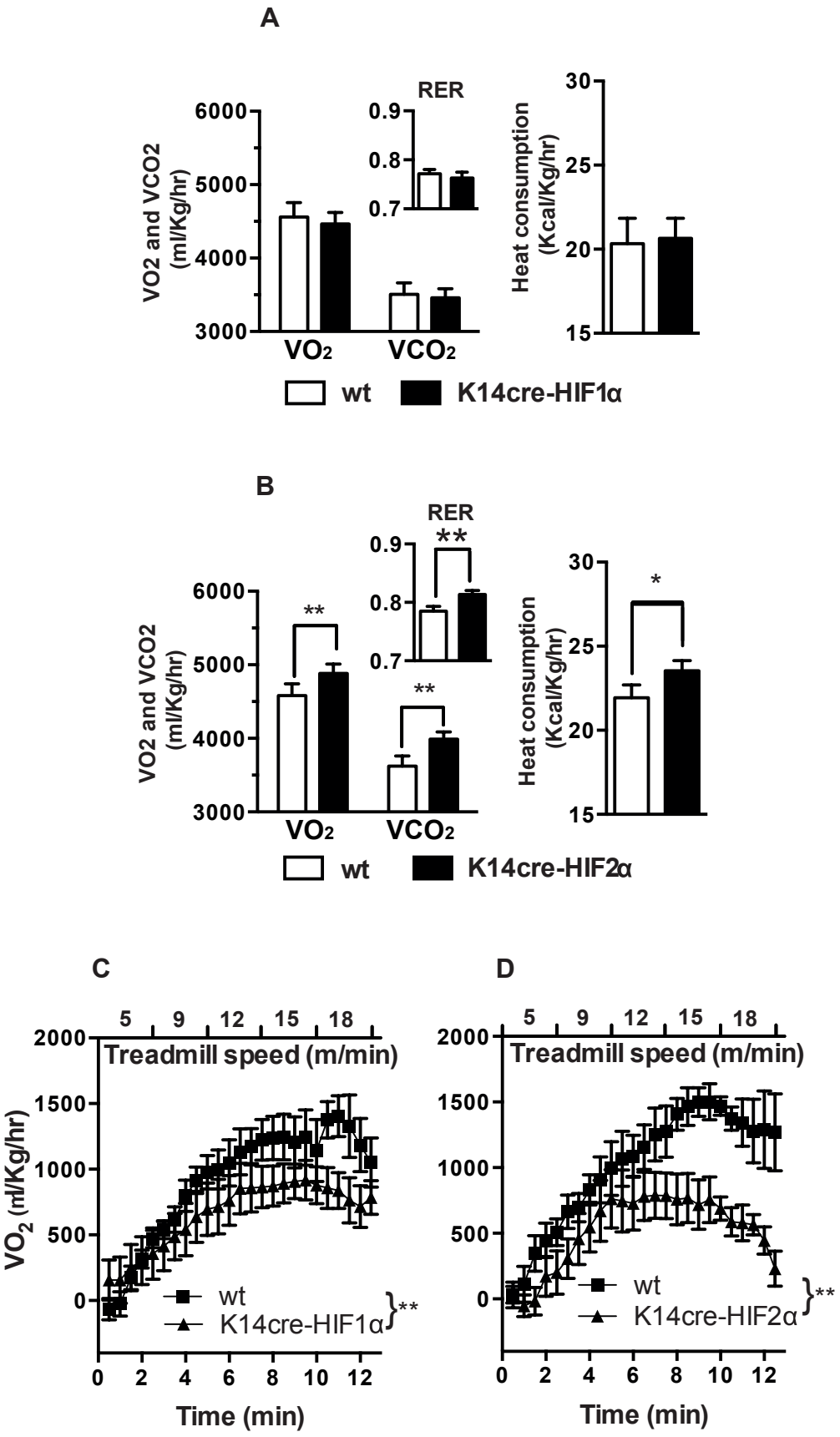


**Figure. S4**. Metabolic characterization of K14cre-HIF-1α and K14cre-HIF-2α. Measurement of VO2 and VCO2 from resting (A) K14cre-HIF-1α or (B) K14cre-HIF-2α mice (data shown as mean VO2 or VCO2 ± SEM ml/Kg/hr), respiratory exchange ration (RER) (data shown as mean ratio ± SEM) and metabolic heat production (data shown as mean Kcal/Kg/h ± SEM) (n=5) (*p<0.05, **p<0.005). (C and D) Whole-body O2 consumption (VO2) in response to accumulating exercise stress. (C) K14-HIF-1α (n=5) or (D) K14-HIF-2α (n=5) were compared to littermate controls (n=4) (anova **p<0.005). Data shown are mean VO2 ± SEM ml/Kg/hr accumulating with time as the intensity of the exercise increases.

Fig. S6

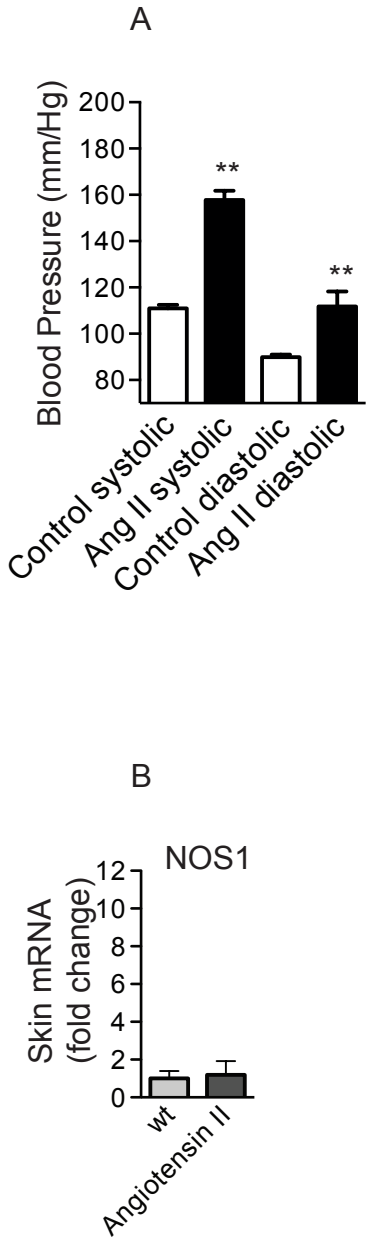


**Figure. S6.** Angiotensin II (2ug/kg/min) infusion in wt over 14 days drives hypertension. (A) WT mice develop severe hypertension (data shown as mean (mm/Hg) ± SEM, n=6). (B) NOS1 mRNA expression remained stable during angiotensin II infusion. (data shown as mean (fold change) ± SEM, n=6

Fig. S7

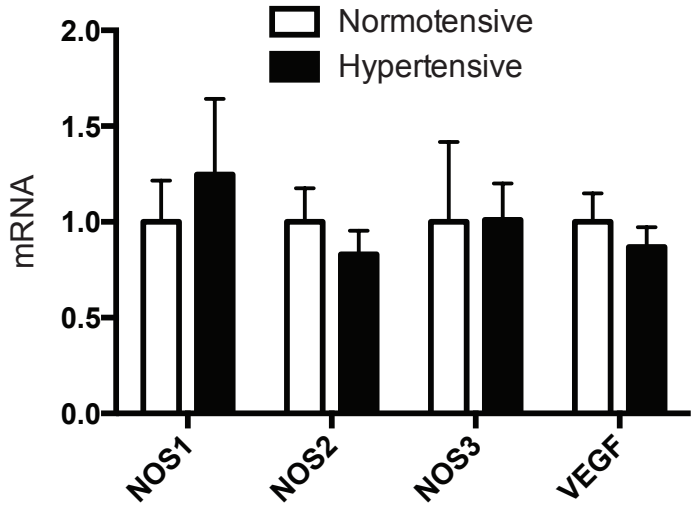


**Figure. S7.** QPCR analysis of NOS1, NOS2, NOS3 and VEGF from skin samples collected from normotensive (open bar n=11) and mildly hypertensive (closed bar n=13) volunteers. Data shown are mean fold change ± SEM.

Fig. S5

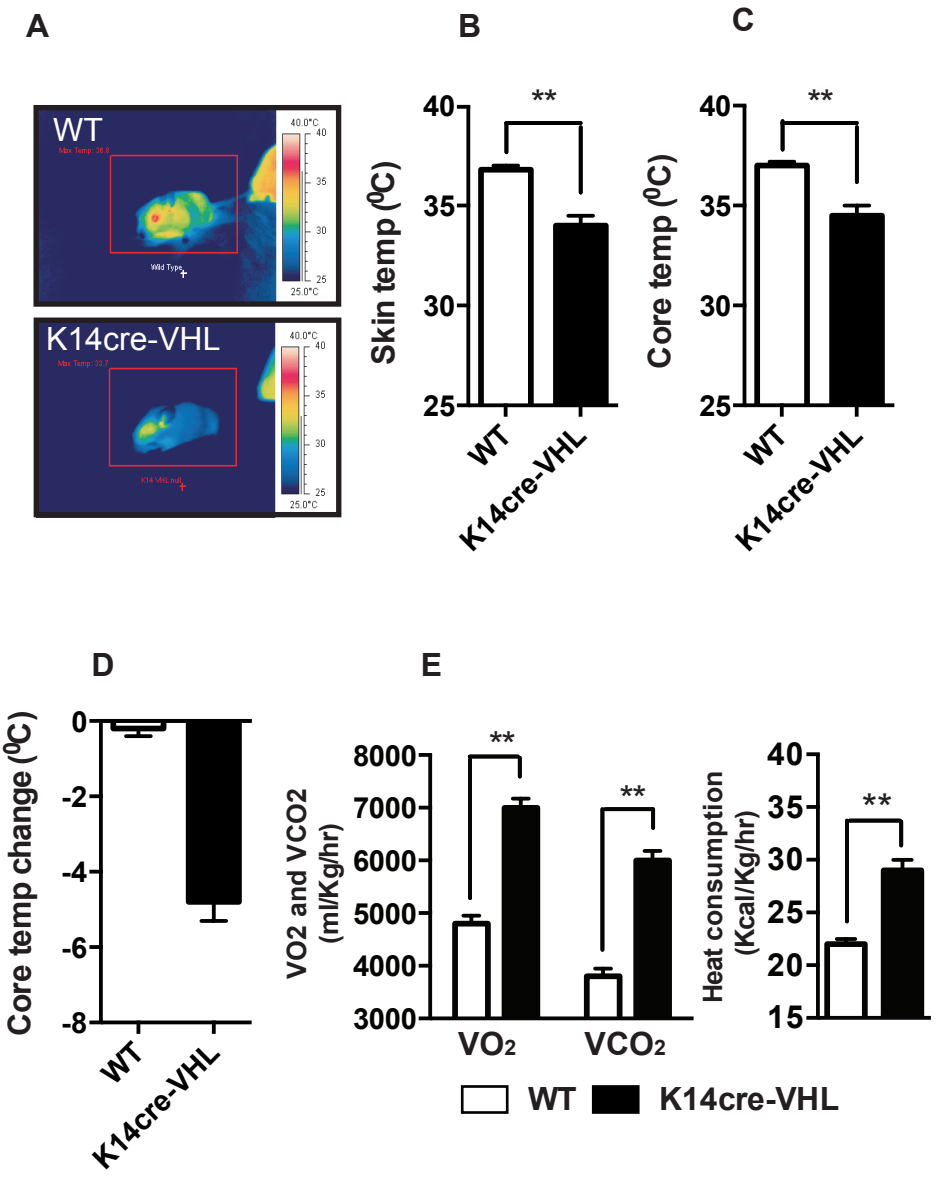


**Figure. S5**. K14cre-VHL mice are hypothermic. (A-B) Skin surface temperature was measured by a thermal infrared camera and expressed as average temperature (oC) ± SEM (n=8). (C) Core-body temperature was monitored during acclimation of K14cre-VHL to 4oC environmental temperature compared to wild-type controls. Data shown as the mean drop in core temperature (oC) ± SEM following 3h exposure (n=8). Measurement of VO2 and VCO2 from resting K14cre-VHL mice (Data shown as mean VO2 or VCO2 ± SEM ml/Kg/hr), metabolic heat production (Data shown as mean Kcal/Kg/h ± SEM) (n=8)(**p<0.005)

Table S1

Mouse Blood Chemistry

| K14-HIF-1α | | | Cre- | Cre+ |
|---|---|---|---|---|
| | | Range | Mean | Mean |
| Glucose | mg/dl | (90-192) | 172.5 | 195.7 |
| BUN | mg/dl | (18-29) | 24 | 23.6 |
| Creatinine | mg/dl | (0.2-0.8) | <0.2 | <0.2 |
| Albumin | g/dl | (2.5-4.8) | 3.6 | 3.8 |
| Globulin | g/dl | - | 2 | 2 |
| Total protein | g/dl | 3.6-6.6) | 6.0 | 6.2 |
| Sodium | mEg/L | (126-182) | 149.6 | 151.75 |
| Potassium | mWg/L | (4.7-6.4) | 6.5 | 7.0 |
| Calcium | mg/dl | (5.9-9.4) | 10.1 | 10.1 |
| Phosphorus | mg/dl | (6.1-10.1) | 6.95 | 6.20 |
| Bilirubin total | mg/dl | (0.1-0.9) | 0.3 | 0.3 |
| SGPT (ALT) | U/L | (28-132) | 42.75 | 42 |
| Alk P | U/L | (62-209) | 52 | 49 |
| Amylase | U/L | (1691-3615) | 1019 | 987 |

**Table S1.** Murine blood chemistry analysis, comparing K14cre-HIF1α with littermate control (n=10)

Table. S2

Subject information

| Subject | Age | Gender | BP at visit | Hypertensive medication | Other medication |
|---|---|---|---|---|---|
| 1 | 46 | F | 144/71 | Candersartan | Nil |
| 2 | 28 | M | 141/96 | Losartan | Nil |
| 3 | 61 | M | 150/85 | Perindopril, Felodipine | Simvastatin, Lanzoprazole |
| 4 | 67 | M | 169/82 | Lisinopril, Doxazocin | Nil |
| 5 | 48 | M | 142/89 | Not yet started | Nil |
| 6 | 50 | M | 167/109 | Nil | Nil |
| 7 | 62 | M | 173/94 | Nil | Nil |
| 8 | 51 | M | 165/99 | Rampril, Amiodipine | Nil |
| 9 | 65 | F | 173/98 | Lisinopril | Latanoprost, Viscotear |
| 10 | 53 | M | 140/90 | Candersartan | Simvastatin, Aspirin |
| 11 | 51 | F | 159/96 | Candersartan | Nil |
| 12 | 70 | M | 150/73 | Not yet started | Simvastatin, Aspirin |
| 13 | 68 | F | 133/66 | Bendroflumethiazide | Pravastatin, Declofenac |
| 14 | 58 | M | 134/82 | Amiodipine, Atenolol | Simvastatin, Aspirin |
| 15 | 56 | M | 173/105 | Nil | Nil |
| 16 | 63 | F | 172/70 | Lisinopril | Nil |
| 1 | 74 | F | 157/86 | Nil | Aspirin |
| 2 | 60 | F | 147/84 | Nil | Nil |
| 3 | 32 | F | 98/73 | Nil | Nil |
| 4 | 51 | M | 124/71 | Nil | Lansoprazole, Aspirin |
| 5 | 24 | M | 98/73 | Nil | Nil |
| 6 | 49 | F | 105/57 | Nil | Nil |
| 7 | 48 | M | 147/86 | Nil | Nil |
| 8 | 47 | F | 116/72 | Nil | Nil |
| 9 | 38 | F | 133/70 | Nil | Nil |
| 10 | 56 | M | 138/83 | Nil | Nil |
| 11 | 43 | F | 113/69 | Nil | Nil |
| 12 | 59 | F | 123/67 | Nil | Nil |
| 13 | 37 | F | 113/56 | Nil | Nil |
| 14 | 54 | F | 106/67 | Nil | Nil |
| 15 | 52 | M | 125/85 | Nil | Nil |
| 16 | 52 | M | 119/70 | Nil | Nil |
| 17 | 50 | F | 122/74 | Nil | Nil |
| 18 | 49 | M | 139/91 | Nil | Nil |
| 19 | 47 | F | 135/80 | Nil | Nil |
| 20 | 48 | M | 150/86 | Nil | Nil |
| 21 | 62 | F | 155/81 | Nil | Nil |
| 22 | 52 | F | 114/58 | Nil | Nil |
| 23 | 23 | F | 103/58 | Nil | Nil |
| 24 | 61 | M | 143/76 | Nil | Nil |

**Table S2.** Human volunteer data.
Subjects are divided into Normotensive and hypertensive subjects